Heat Transfer Research 49(10):949–964 (2018)

NUMERICAL INVESTIGATION OF MIXED CONVECTION OF SiO_2–WATER NANOFLUIDS WITHIN AN INCLINED DOUBLE LIDS-DRIVEN CAVITY

J. Amani,[1] D. Toghraie,[2,] A. Karimipour,[3] A. Niroumand,[4] & M.R. Faridzadeh[3]*

[1]*Department of Mechanical Engineering, Isfahan University of Technology, Isfahan, Iran*

[2]*Department of Mechanical Engineering, Khomeinishahr Branch, Islamic Azad University, Khomeinishahr, Iran*

[3]*Department of Mechanical Engineering, Najafabad Branch, Islamic Azad University, Najafabad, Iran*

[4]*Department of Mechanical Engineering, University of Kashan, Kashan, Iran*

*Address all correspondence to: Davood Toghraie, E-mail: Toghraee@iaukhsh.ac.ir

Original Manuscript Submitted: 3/27/2013; Final Draft Received: 2/9/2016

To investigate mixed convection flows through nanofluid in a square double lid-driven cavity with various inclination angles, a numerical method based on the finite volume approach was applied. In this study, a SiO_2–water nanofluid was used. The cavity was nonuniformly heated from the left, T_h, and cooled from the opposite wall. The top and the bottom moving walls were insulated. The study was conducted for the Richardson number 0.1 to 10, Reynolds number 1 to 100, with solid volume fractions (φ) of nanoparticles being altered from 0 to 0.06. The Patel and Brinkman models were used for calculating thermal conductivity and effective viscosity of the nanofluid, respectively. The impact of Reynolds number, Richardson number, inclination of cavity, and of solid volume fraction of the nanofluid on the hydrodynamic and thermal characteristics were studied and discussed. As a result, it was found that the heat transfer rate increases with solid volume fraction.

KEY WORDS: *mixed convection, double lid-driven, nanofluid, nonuniform heating, cavity, numerical study*

1. INTRODUCTION

Until today, people have made efforts to enhance convective heat transfer by means of surface enlargement using obstacles such as ribs and fins and the increase in flow turbulence due to the interaction between the flow and the obstacles. However, additional pressure losses increase with introduction of obstacles and turbulence. The low thermal conductivity of conventional fluids such as water, oil, and of an ethylene glycol mixture is a serious limitation on improving the performance and compactness of this engineering equipment. To overcome the above-mentioned disadvantages, there is a strong motivation to develop advanced heat transfer fluids with substantially higher conductivity. An innovative way of improving the thermal conductivities of fluids is to suspend small solid particles in a fluid. Nanofluids are new heat transfer fluids containing a small quantity of nano-sized particles that are uniformly and stably suspended in a liquid. The dispersion of a small amount of solid nanoparticles in conventional fluids remarkably changes their thermal conductivity. Compared to the existing techniques for enhancing heat transfer, the nanofluids show a superior potential for increasing heat transfer rates in a variety of cases. In addition, flow in a lid-driven cavity or in a two-sided

NOMENCLATURE

A	heat transfer area, m^2
c_p	constant pressure specific heat, J/kg·K
d_f	molecular size of liquid, m
d_p	particle diameter, m
g	gravitational acceleration, m/s^2
h	heat transfer coefficient, $W/m^2 \cdot K$
k	thermal conductivity, W/m·K
k_b	Boltzmann constant, $1.3806503 \times 10^{-23}$ kg·m^2·K^{-1}·s^{-2}
L	cavity length, m
Nu	local Nusselt number, hL/k_f
Nu_m	average Nusselt number
p	pressure, Pa
P	dimensionless pressure, $p/\rho_{nf}u_0^2$
Pe	Peclet number, $u_p d_p/\alpha_f$
Pr	Prandtl number, υ_f/α_f
q''	heat flux, W/m^2
Ra	Rayleigh number, $(g\beta_f \Delta T L^3)/(\upsilon_f \alpha_f)$
Re	Reynolds number, $(\rho_f u_0 L)/\mu_f$
Ri	Richardson number, $Ra \cdot Pr^{-1} \cdot Re^{-2}$
T	temperature, K
ΔT	$T_h - T_c$, K
u_o	lid velocity, m/s
u_p	Brownian motion velocity of nanoparticle
u, v	velocity components in (x, y) direction, m/s
U, V	dimensionless velocity, u/u_o, v/u_o
x, y	global Cartesian coordinates, m
X, Y	dimensionless Cartesian coordinates, x/L, y/L

Greek symbols

α	thermal diffusivity, m^2/s
β	thermal expansion coefficient, 1/K
γ	inclination angle, Fig. 1
μ	dynamic viscosity, kg·m^{-1}·s^{-1}
ν	kinematic viscosity, m^2/s
ρ	density, kg/m^3
θ	dimensionless temperature, $(T - T_c)/(T_h - T_c)$
φ	solid volume fraction

Subscripts

c	cold wall
f	pure fluid
h	hot wall
m	average Nusselt number
nf	nanofluid
p	particle

lid-driven enclosure can be used in certain engineering applications such as electronic devices cooling, lubrication technologies, furnaces, chemical processing equipment, drying technologies, etc. Heat transfer and fluid flow properties have been studied previously in some of the works for rectangular or square cavities driven by buoyancy and shear forces. Oztop and Dagtekin (2004) investigated a mixed convection problem in a vertical two-sided lid-driven differentially heated square cavity by a numerical method. The left and right moving walls were maintained at different constant temperatures, and the top and bottom walls were thermally insulated. The results have showed that both the Richardson number and the direction of the moving walls affect the fluid flow and heat transfer in the cavity. Luo and Yang (2007) have presented an extension of the method of calculating flow bifurcation with/without heat transfer in a cavity with opposite movement of top and bottom walls. Ouertatani et al. (2009) studied three-dimensional flow structures and heat transfer

rates in air within double lid-driven cubic cavity heated from the top and cooled from below numerically. The other walls were maintained adiabatic. They obtained that a remarkable heat transfer improvement of up to 76% can be reached for the case of Re = 400 and Ri = 1. Wahba (2009) simulated incompressible flow in two-sided and four-sided lid-driven cavities by a numerical method. For the two-sided lid-driven cavity, the upper wall moved to the right while the left wall moved downward with the speeds equal to that of the upper wall. At low Reynolds numbers, the flow field was symmetric with respect to one of the cavity diagonals for the two-sided lid-driven cavity, while for the four-sided lid-driven cavity, it proved to be symmetric with respect to both cavity diagonals. Many engineering electronic devices and mechanical instruments were limited by enhancing the performance and heat transfer rate in conventional fluids such as water, oil, and ethylene glycol mixtures. Primarily, of the reason is the low thermal conductivity of the active fluid. There are several procedures to develop heat transfer of fluids. An innovative way is improving the thermal conductivities of the active fluid by adding metallic nanoparticles to it, namely, the nanofluid, and consequently enhancing the heat transfer characteristics. In order to calculate the nanofluid properties, many models have been developed for estimating the thermal conductivity of nanofluids based on several parameters such as the geometry of nanoparticles, Brownian effects, temperature and interaction between nanoparticles and the base fluid (Karimipour, 2015; Zarringhalam et al., 2016; Esfe et al., 2015a; Akbari et al., 2016).

Maxwell (1904) proposed the first model for low-density mixtures with spherical particles. Based on the Maxwell model, the thermal conductivity of a nanofluid increases with increase in the volume fraction of solid nanoparticles. Many researchers investigated heat transfer and flow characteristics of a nanofluid in lid-driven enclosures (Karimipour et al., 2014; Eshgarf and Afrand, 2016; Esfe et al., 2014). Tiwari and Das (2007) numerically investigated the behavior of a copper–water nanofluid within a two-sided lid-driven differentially heated square cavity. The upper and bottom walls were insulated and the left and the right moving walls were maintained at constant temperatures. Three cases were studied based on the direction of movement of the walls. They found that the Richardson number, depicting the direction of the moving walls, affects the heat transfer and fluid flow in the cavity. Noor et al. (2009) investigated flow and heat transfer inside a square cavity with oscillating double side by a numerical procedure. Sivasankaran et al. (2010) performed a numerical study of mixed convection in a lid-driven cavity at different Prandtl numbers. The vertical sidewalls of the cavity were maintained with sinusoidal temperature distribution. The results showed that the heat transfer rate increased with the increasing amplitude ratio. It was observed that average Nusselt numbers were increased first, and then decreased when the phase deviation increased from 0 to π. The mixed convection heat transfer process, observed in double lid-driven cavities, is important in industrial applications and engineering designs. In many applications, the angle of cavity changes intentionally or involuntarily. Based upon the angle of the cavity, the lid-driven shear force may assist or oppose the buoyancy force and change the heat transfer rates. In addition, in order to enhance the heat transfer rate, an innovative technique replaces an active fluid by a nanofluid. Thus, in this paper, numerical study was performed in a SiO_2–water nanofluid within a square double lid-driven cavity with stationary cooled right wall and heated sinusoidal left wall. The diameter of the nanoparticles is assumed to be 100 nm. Since the nanofluid consists of very small-sized solid particles, at low solid concentration, it is reasonable to consider the nanofluid as a single-phase flow (Xuan and Li, 2000). The results were presented in the form of the stream contours, isotherm lines, and average Nusselt number. The purpose of this note is to enhance the discussion on the use of nanofluids with the sole aim of increasing the heat transfer coefficient in mixed convection flows in a square double lid-driven cavity with various inclination angles. The obtained results may have direct applications in industrial processes and technologies such as furnaces, lubrication technologies, drying technologies, chemical processing

equipment, and others. More recent works can be referred to those involving nanofluid flow and heat transfer as like (Karimipour et al., 2011, 2015; Esfe et al., 2015b,c; Nikkhah et al., 2015; Akbari et al., 2015).

2. PROBLEM STATEMENT

Figure 1 shows a two-dimensional square double lid-driven cavity filled with a SiO_2–water nanofluid. The cavity is heated sinusoidally from the left wall and cooled from the right wall. Both top and bottom moving walls were thermally insulated. The cavity is subjected to top and bottom driven lids, and filled with a suspension of SiO_2 nanoparticles in water, with the diameters of nanoparticles equal to 100 nm. Since the nanofluid consists of very small solid particles, in low solid concentration, it is reasonable to consider the nanofluid as a single-phase flow.

Table 1 presents the thermophysical properties of water and SiO_2 at the reference temperature. It is assumed that the base fluid and the nanoparticles are in thermal equilibrium, and that there is no slip between

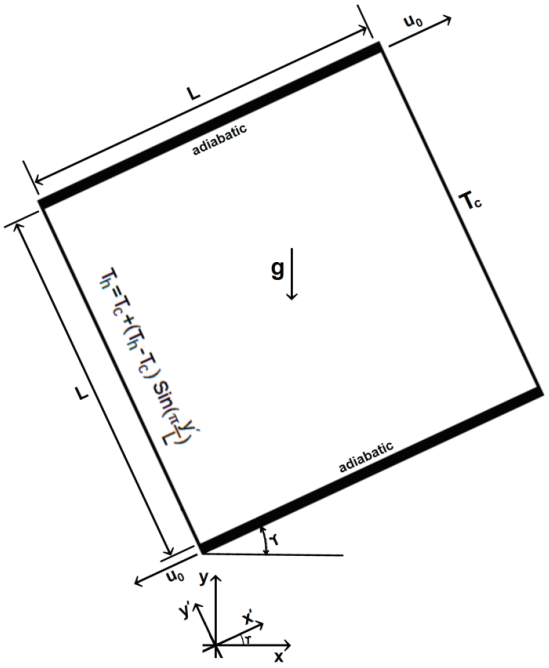

FIG. 1: Schematic diagram of the physical system

TABLE 1: Thermophysical properties of different phases

Physical Properties	Fluid Phase (water)	Solid (SiO_2)
c_p, J/kg·K	4179	765
ρ, kg/m^3	997.1	3970
k, W·m^{-1}·K^{-1}	0.6	36
$\alpha \times 10^5$	1.47	118.536
$\beta \times 10^5$, 1/K	21	0.63
$\mu \times 10^4$, kg/m·s	8.9	—

them, and the shape and size of solid particles are uniform. Except for the density, the properties of the nanoparticles and fluid are taken to be constant. In addition, we neglect the viscous dissipation in the governing equations.

3. GOVERNING EQUATIONS

The governing equations for the steady, 2D laminar and incompressible mixed convection flow are expressed as follows:

$$\frac{\partial u}{\partial x'} + \frac{\partial v}{\partial y'} = 0\,, \tag{1}$$

$$u\,\frac{\partial u}{\partial x'} + v\,\frac{\partial u}{\partial y'} = -\,\frac{1}{\rho_{nf}}\,\frac{\partial p}{\partial x'} + \upsilon_{nf}\nabla^2 u + \frac{(\rho\beta)_{nf}}{\rho_{nf}}\,g\,\sin\,(\gamma)(T - T_c)\;, \tag{2}$$

$$u\,\frac{\partial v}{\partial x'} + v\,\frac{\partial v}{\partial y'} = -\,\frac{1}{\rho_{nf}}\,\frac{\partial p}{\partial y'} + \upsilon_{nf}\nabla^2 v + \frac{(\rho\beta)_{nf}}{\rho_{nf}}\,g\,\cos\,(\gamma)(T - T_c)\,, \tag{3}$$

$$u\,\frac{\partial T}{\partial x'} + v\,\frac{\partial T}{\partial y'} = \alpha_{nf}\nabla^2 T\,. \tag{4}$$

The following dimensionless parameters are used to obtain the dimensionless form of the governing equations:

$$X = \frac{x'}{L}\,,\quad Y = \frac{y'}{L}\,,\quad V = \frac{v}{u_0}\,,\quad U = \frac{u}{u_0}\quad,\quad \Delta T = T_h - T_c,\quad \theta = \frac{T - T_c}{\Delta T}\,,\quad P = \frac{p}{\rho_{nf}u_0^2}\,, \tag{5}$$

where T_h is the maximum temperature of the left wall surface calculated from the definition of the Ra number. Reynolds number and other parameters are defined as follows:

$$\mathrm{Re} = \frac{\rho_f u_0 L}{\mu_f}\,,\quad \mathrm{Pr} = \frac{\upsilon_f}{\alpha_f}\,,\quad \mathrm{Ra} = \frac{g\mathrm{B}_f\Delta T L^3}{\upsilon_f\alpha_f}\,,\quad \mathrm{Gr} = \frac{\mathrm{Ra}}{\mathrm{Pr}}\,,\quad \mathrm{Ri} = \frac{\mathrm{Gr}}{\mathrm{Re}^2}\,. \tag{6}$$

The thermal diffusivity and effective density of the nanofluid are given by

$$\alpha_{nf} = \frac{k_{nf}}{(\rho c_p)_{nf}}\,, \tag{7}$$

$$\rho_{nf} = \varphi\rho_p + (1 - \varphi)\rho_f\,. \tag{8}$$

The heat capacitance and the thermal expansion coefficient of the nanofluid are defined as

$$(\rho c_p)_{nf} = \varphi(\rho c_p)_p + (1 - \varphi)(\rho c_p)_f\,, \tag{9}$$

$$(\rho\beta)_{nf} = \varphi(\rho\beta)_p + (1 - \varphi)(\rho\beta)_f\,. \tag{10}$$

The viscosity of the nanofluid is estimated by using the Brinkman model given by

$$\mu_{nf} = \frac{\mu_f}{(1-\varphi)^{2.5}}. \tag{11}$$

Several relations can be used for the expression of the effective thermal conductivity of the nanofluid. In this study, the model of Patel et al. (2005) is used to determine the thermal conductivity of the nanofluid:

$$\frac{k_{nf}}{k_f} = 1 + \frac{k_p A_p}{k_f A_f} + c k_p Pe \frac{A_p}{k_f A_f}. \tag{12}$$

The parameter c is equal to 25,000. Other parameters used are defined here as

$$\frac{A_p}{A_f} = \frac{d_f}{d_p}\frac{\varphi}{1-\varphi}, \quad \mathrm{Pe} = \frac{u_p d_p}{\alpha_f}, \quad u_p = \frac{2k_b T}{\pi \mu_f d_p^2} \quad d_p = 100\ \mathrm{nm}, \quad d_f = 2.\text{Å}. \tag{13}$$

In order to investigate the effects of different parameters on heat transfer, the local Nusselt number is defined as follows:

$$\mathrm{Nu} = \frac{hL}{k_f}, \tag{14}$$

where the heat transfer coefficient is

$$h = \frac{q''}{T_h - T_c}. \tag{15}$$

The value of the heat flux over the cold wall is expressed as

$$q'' = -k_{nf}\frac{\partial T}{\partial x'}. \tag{16}$$

By substituting Eqs. (15) and (16) into Eq. (14), the local Nusselt number can be written as

$$\mathrm{Nu} = -\frac{k_{nf}}{k_f}\frac{\partial \theta}{\partial X}. \tag{17}$$

The average Nusselt number over the cold surface is expressed as follows:

$$\mathrm{Nu}_m = \frac{1}{L}\int_0^L \mathrm{Nu} dy'. \tag{18}$$

The boundary conditions are as follows:

left wall:
$$\begin{cases} U = V = 0 \\ T(y') = T_c + (T_h - T_c)\sin\left(\dfrac{\pi y'}{L}\right) \rightarrow \theta = \sin(\pi Y); \end{cases} \tag{19}$$

right wall:
$$\begin{cases} U = V = 0 \\ \theta = 0 \end{cases}; \tag{20}$$

$$\text{top wall:} \quad \begin{cases} U = 1, \quad V = 0 \\ \dfrac{\partial \theta}{\partial Y} = 0 \end{cases}; \tag{21}$$

$$\text{bottom wall:} \quad \begin{cases} U = -1, \quad V = 0 \\ \dfrac{\partial \theta}{\partial Y} = 0 \end{cases}. \tag{22}$$

4. NUMERICAL METHOD

The continuity, momentum, and energy balance equations have been solved using the control-volume numerical code and the SIMPLER algorithm (Brinkman, 1958) used for the pressure–velocity coupling. In order to assess the accuracy of the results, a complete study has been carried out with the use of Basak et al.'s (2009) model. Figure 2 shows some results in the form of temperature contours for the uniform bottom heating case with Re = 100, Gr = 10^4, Pr = 0.7 (left figure) and Pr = 10 (right figure). The diagrams are in accordance.

To study the effect of the grid size on the results, two cases were investigated by changing the number of grid points in uniform mesh. The results of this study are presented in Table 2 for various cases. Grid independence was achieved within the grid size of 121 × 121.

5. RESULTS AND DISCUSSION

For extreme combinations of high Ri and low Re numbers, heat transfer is substantially dominated by conduction. For extreme combinations of small Ri and high Re numbers, the dominant heat transfer becomes convective. In this paper, natural and forced convection were investigated. The top and bottom walls were adiabatic moving to right and left, respectively. The left wall had a sinusoidal temperature and the right wall had a low temperature T_c. The stream function, isotherm lines, and the average Nusselt number were presented for the SiO_2–water nanofluid for $0.1 < Ri < 10$, $1 < Re < 100$, $0.0 < \varphi < 0.06$, and $0^o < \gamma < 150^o$.

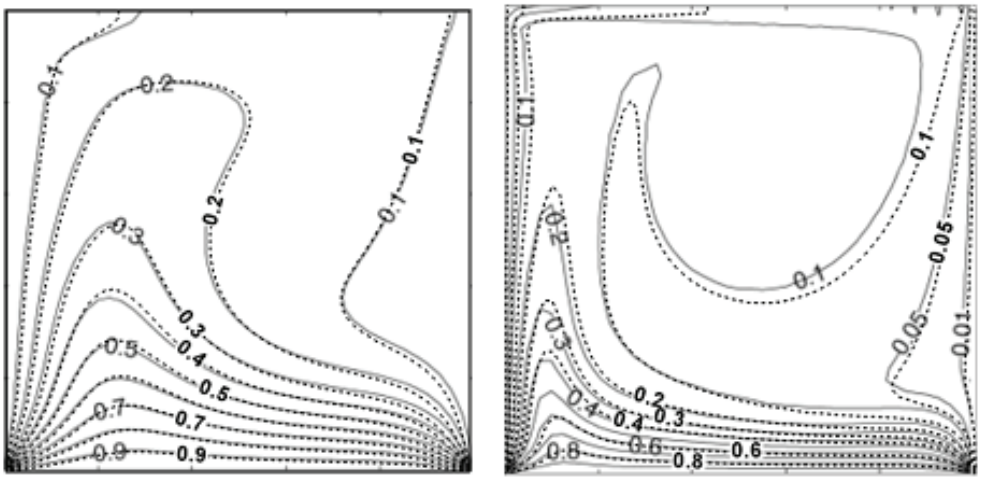

FIG. 2: Temperature contours for uniform bottom heating case with Re = 100, Gr = 104, Pr = 0.7 (left figure) and Pr = 10 (right figure) for current study (….) and Basak et al. (2009) (—)

TABLE 2: Nu_m values for two different cases for finding the optimum mesh

$\varphi = 0.06$, Re = 100, Ri = 10, $\gamma = 150^o$	$\varphi = 0.02$, Re = 1, Ri = 0.1, $\gamma = 0^o$	Mesh Size
5.615	0.709	41 × 41
5.821	0.713	61 × 61
6.089	0.715	77 × 77
6.179	0.716	93 × 93
6.211	0.716	105 × 105
6.225	0.717	121 × 121
6.232	0.717	141 × 141

Figure 3 presents streamlines and temperature field for Ri = 2 for both the base fluid ($\varphi = 0$) and nanofluid ($\varphi = 0.06$). It is observed that a single recirculation eddy dominates the cavity. The intensity of streamlines near the moving walls is high, and a vertical circulation is created in the center of the enclosure. By increasing the Reynolds number from 1 to 100, the nanofluid moves faster in the horizontal direction, the width of the vertical circulation increases, and the streamlines accede to the hot and cold surfaces and thus, heat transfer increases because of the enhancement in the rate of flow passing near hot and cold surfaces. For all angles other than 150^o and Re = 100, a single recirculation eddy is observed in the cavity. At $\gamma = 150^o$ and Re = 100 a circulation in the cavity and a small vortex are created at the bottom of the hot wall. Because at $\gamma = 120^o$ and 150^o the heated nanofluid moves upward, while the driven lids cause the movement of the nanofluid in the opposite direction from the buoyancy force, towards the bottom. When the cavity inclination angle changes from zero to 150^o, the circulation flow in the cavity becomes weaker. Increment in solid volume fraction does not cause noticeable changes in the streamline contours, but streamlines in some cases at Re = 100 approach the left and right walls. At Re = 100 and $\gamma = 150^o$, by increasing the solid volume fraction, the size of the small vortex decreases and streamlines approach the wall surfaces.

The form of the isotherm lines near the hot wall is due to the sinusoidal distribution of temperature on a heat source. The isotherm line has such a form because the temperature in the center of the hot wall is at its highest value and has the lowest value near the top and bottom wall. The nanofluid beside the hot wall expands and moves towards the upper wall due to the buoyancy force. As mentioned before, the upper part of the hot wall has a lower temperature than the middle of the wall. So, the finally heated nanofluid faces the part of the wall with a lower temperature, and this leads to the transfer of the amount of heat from the hot nanofluid to the wall. Therefore, the amount of net heat transfer of the left wall is reduced. By increasing the Re number at a particular inclination angle and the Richardson number, the temperature gradient near the surface increases. Therefore, the local heat transfer from the middle and top of the hot wall increases and a transaction is created between local heat transfers. For Re = 1, the isotherm lines are almost parallel in the right part of the cavity. In this part of the cavity, there is conductive heat transfer between the vertical layers of the nanofluid, which changes to conductive heat transfer between the horizontal layers near the top and bottom walls by changing the Re number from 1 to 100. By increasing the inclination angle at a lower Reynolds number, small changes in the isotherm lines are observed. Both natural and forced heat transfer are important at Ri = 2. Because of the low Re numbers, the conductive heat transfer dominates. Therefore, the change in the inclination angle does not affect much the temperature lines. At $\gamma = 0^o$, the forces caused by the moving lids and the buoyancy act in the same direction in which the temperature of the heated fluid de-

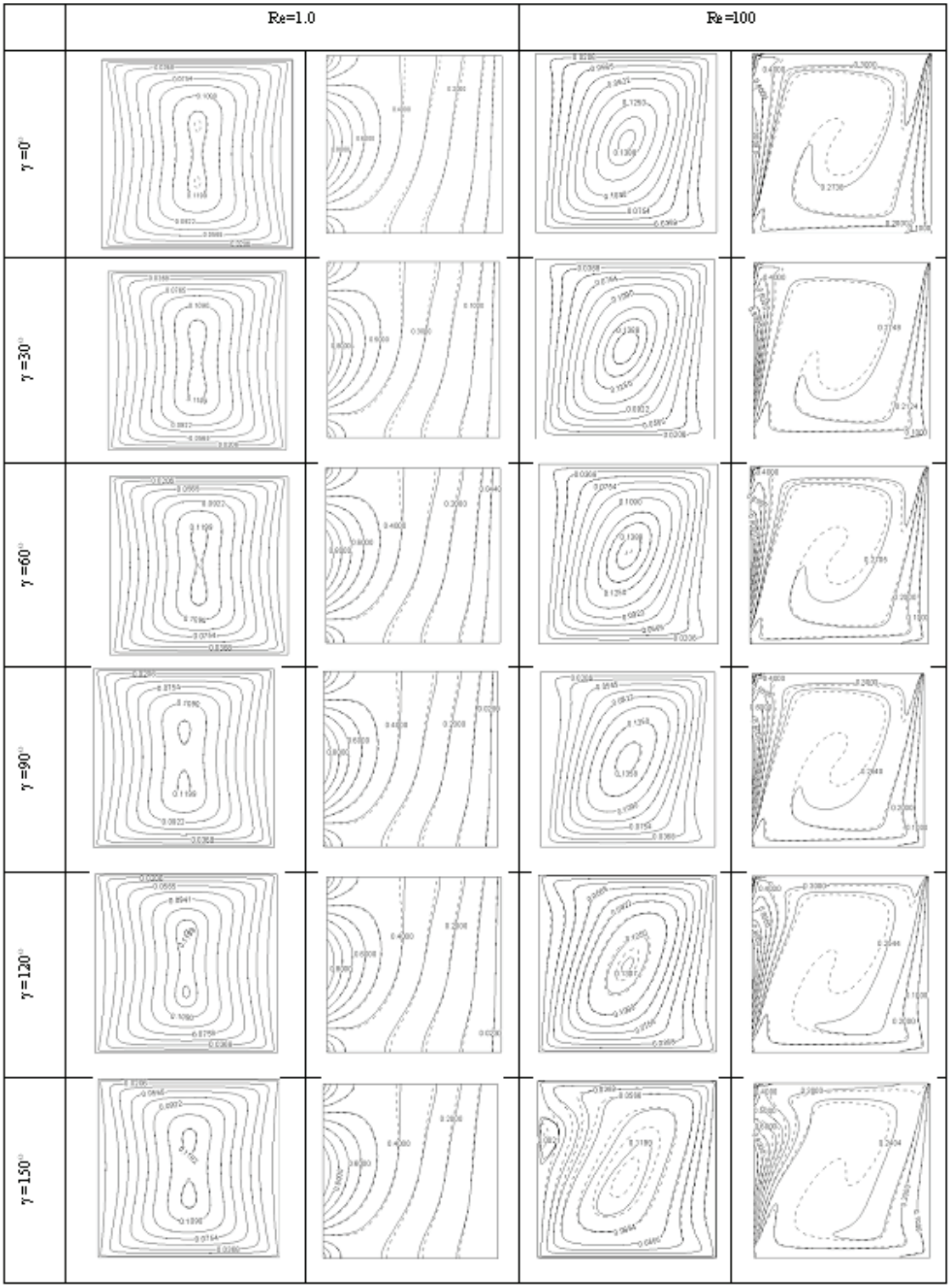

FIG. 3: Flow pattern and thermal fields for Ri = 2, base fluid (—), and nanofluid with φ = 0.06 (- - -)

creases due to its contact with the colder part of the left wall. The buoyancy force always acts in the vertical direction, and the forced convection acts tangentially to the wall surfaces. By increasing γ, the heated nanofluid gets away from the hot wall, which has a lower temperature in comparison with the nanofluid at the upper portion. Therefore, the value of the isotherm lines at a distance from the hot wall increases at a higher inclination angle. This behavior is more obvious at $\gamma = 150^o$. When φ increases from 0 to 0.06, the isotherm lines get closer to the hot heat source surface near the hot or cold walls. Figure 4 shows the streamlines for various Ri and Re numbers for $\gamma = 30^o$. By increasing the Re number from 1 to 100, a stronger flow field is produced in the cavity. When the Ri number is altered from 0.1 to 10, the conduction and natural convection increase. Because the buoyancy and shear forces are aiding each other for $\gamma = 30^o$, the intensity of streamlines increases near the walls and the circulation in the cavity becomes stronger. Increment in φ generally causes stronger circulation.

Isotherm lines are presented in Fig. 5 for $\gamma = 30^o$. With increase in the Re or Ri number, the isotherm lines get closer to the hot and cold walls. Therefore, the temperature gradient increases especially near the cold wall as the heat transfer does. Increment in nanoparticle causes two different behaviors in the isotherm lines. It is observed that some pieces of lines approach the walls but other pieces get away because of the sinusoidal distribution of temperature in the hot wall surface.

Figure 6 presents average Nusselt numbers for all the cases studied. An average Nusselt number has very small variation at very low Re and Ri. At Re = 1, by increasing the Ri number from 0.1 to 10, the values of Nu_m decrease a little for $\gamma = 120^o$ and 150^o, and increase for $\gamma = 0^o$, 30^o, and 60^o. At $\gamma = 90^o$, the values of Nu_m remain constant. At Re = 10, natural convection increases with increasing Ri, and buoyancy force moves the nanofluid upward while forced convection moves the nanofluid near the walls. Thus, the average Nusselt number decreases by increasing the inclination. At Re = 10, Nu_m increases while Ri changes from 0.1 to 10 for $0^o \leq \gamma \leq 120^o$, and decreases at $\gamma = 150^o$. Generally, an enhancement in Nu_m is observed by changing the Ri number from 0.1 to 10 for all γ values at Re = 100. Only a decrease in Nu_m occurs for $\gamma = 150^o$ and 120^o by increasing Ri from 0.1 to 2.

At Re = 1, the values of Nu_m decrease by increasing the inclination angle for all Ri numbers. The highest variation of Nu_m with Ri is observed at $\gamma = 0^o$. Slope of Nu_m–Ri decreases by enhancing γ until a low slope at $\gamma = 120^o$ and then negative slope (decreases in Nu_m) at $\gamma = 150^o$ is observed. The average Nusselt number increases by changing γ from 0^o to 30^o and decreases by more increase in γ for for all Ri numbers and Re = 10. Nu_m increases at Re = 100 by increasing γ from 0^o to 30^o for all Ri numbers and decreases by changing γ from 30^o to 150^o for Ri = 0.1 and 2, and $\gamma = 30^o$ to 90^o for Ri = 7 and 10. By changing the γ value from 90^o to 120^o, it is observed that Nu_m increases extremely and then decreases a little for $\gamma = 150^o$ relative to 120^o. Figure 7 shows streamlines and isotherms for $\gamma = 150^o$, Re = 100, $\gamma = 0.06$, and Ri = 2, Ri = 7, and Ri = 10. According to Fig. 7, three circulations are created in the cavity for Ri = 7 and 10, while at Ri = 2, only one main circulation exists, because at Ri = 2, the buoyancy force is weaker than at Ri = 7 and Ri = 10. Thus, by augmenting the Ri number from 2 to 7 and 10, the buoyancy force causes the fluid to move upward (perpendicular to the surface), while the driven lids cause the fluid to move near the surfaces. Because of the two strong forces, three circulations are created in the cavity, while at Ri = 2, as mentioned, the buoyancy force is weaker than at Ri = 7 as shear forces are created by the driven lids at Ri = 2. Thus, shear forces conquest the buoyancy force and a main circulation in the cavity and a small circulation near the hot surface — in the middle of the wall because of sinusoidal distribution — are created. It is observed from Fig. 7 that by increasing the Ri number, the intensity of temperature lines near the cold wall increases, and the heated fluid rises from the hot surface. Hence, the average Nusselt numbers increase by increasing the nanoparticle volume fraction for all the cases studied.

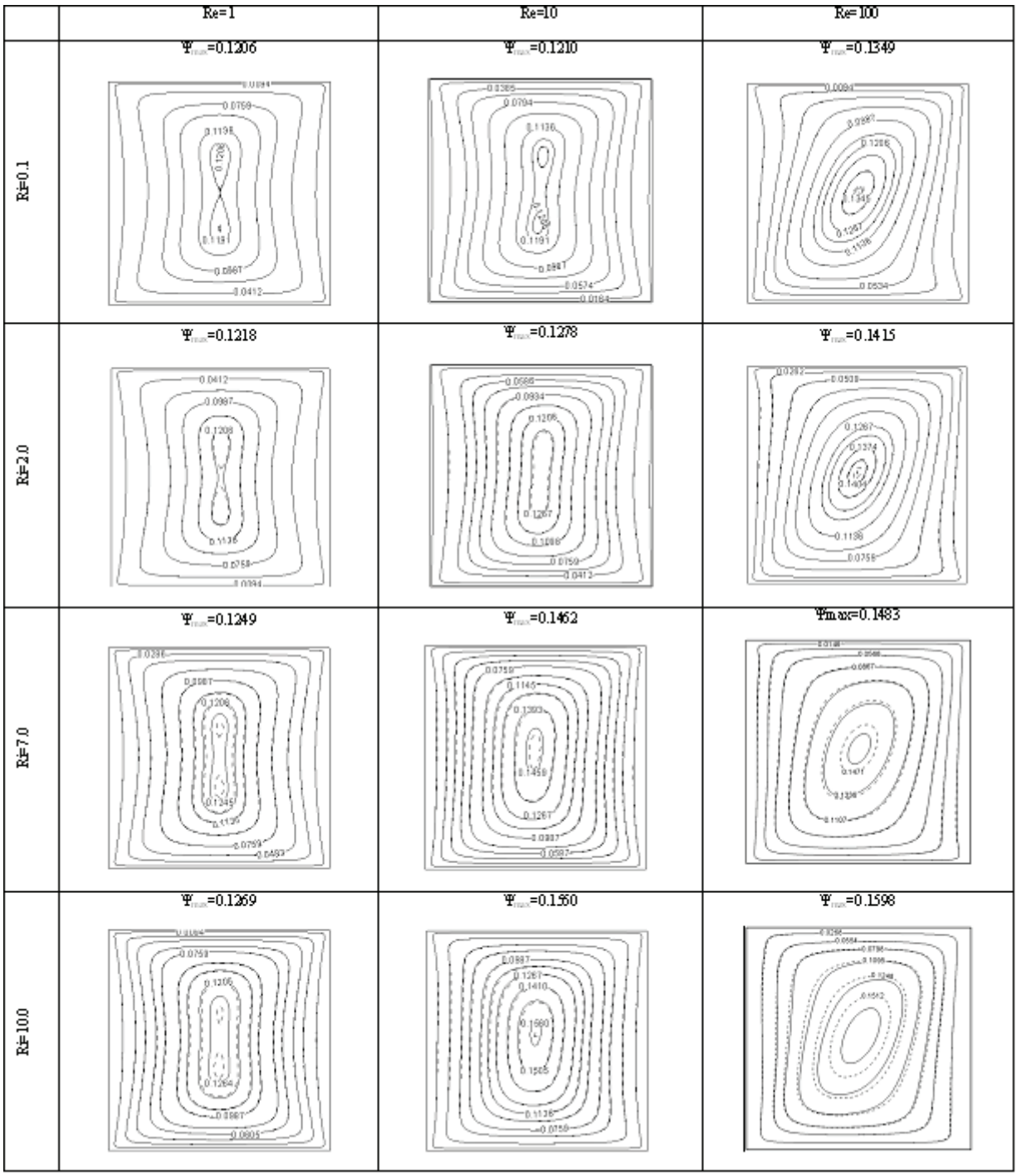

FIG. 4: Flow pattern at $\gamma = 30^{o}$, base fluid (—), and nanofluid with $\varphi = 0.06$ (- - -)

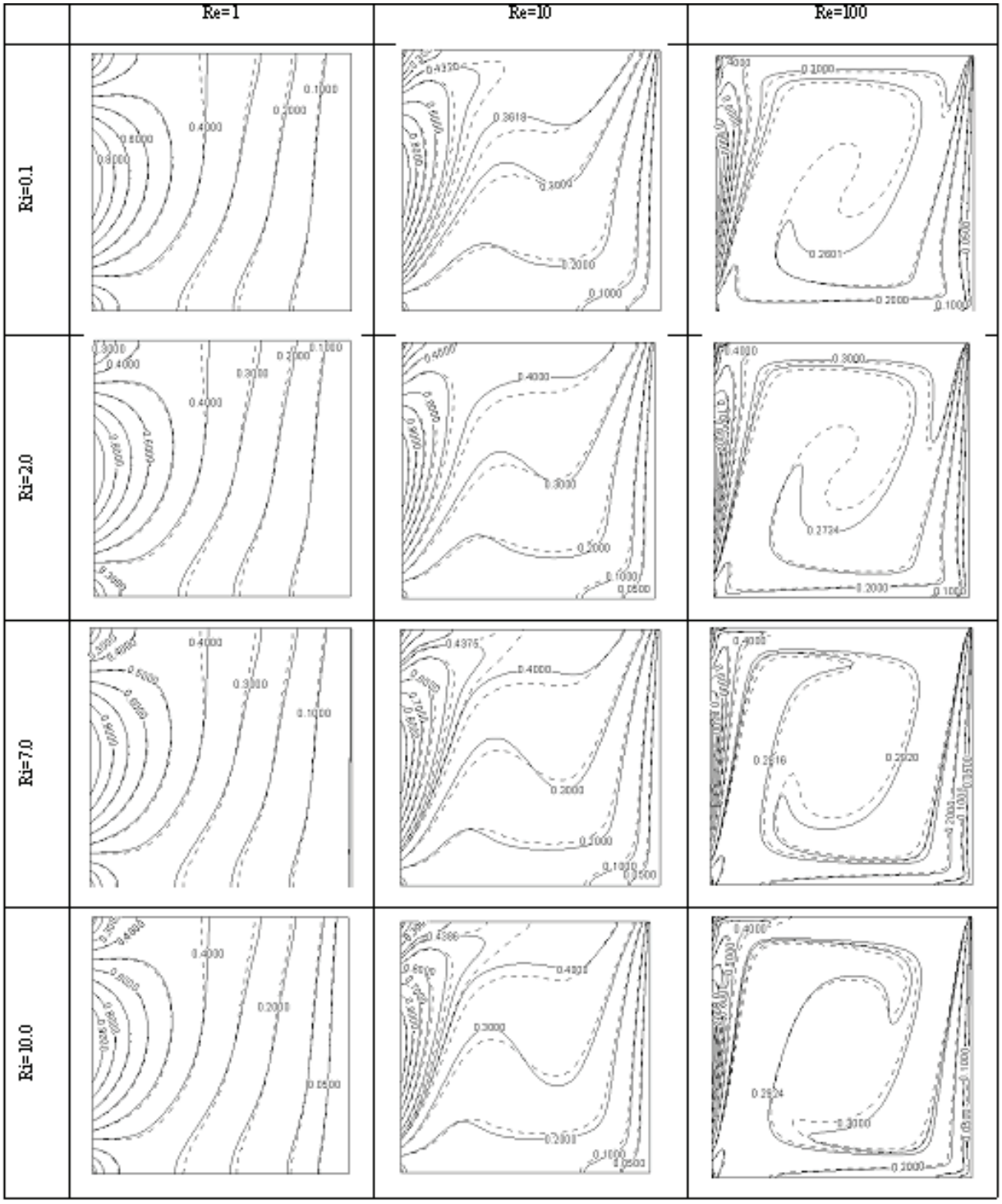

FIG. 5: Thermal fields at $\gamma = 30^{o}$, base fluid (—), and nanofluid with $\varphi = 0.06$ (- - -)

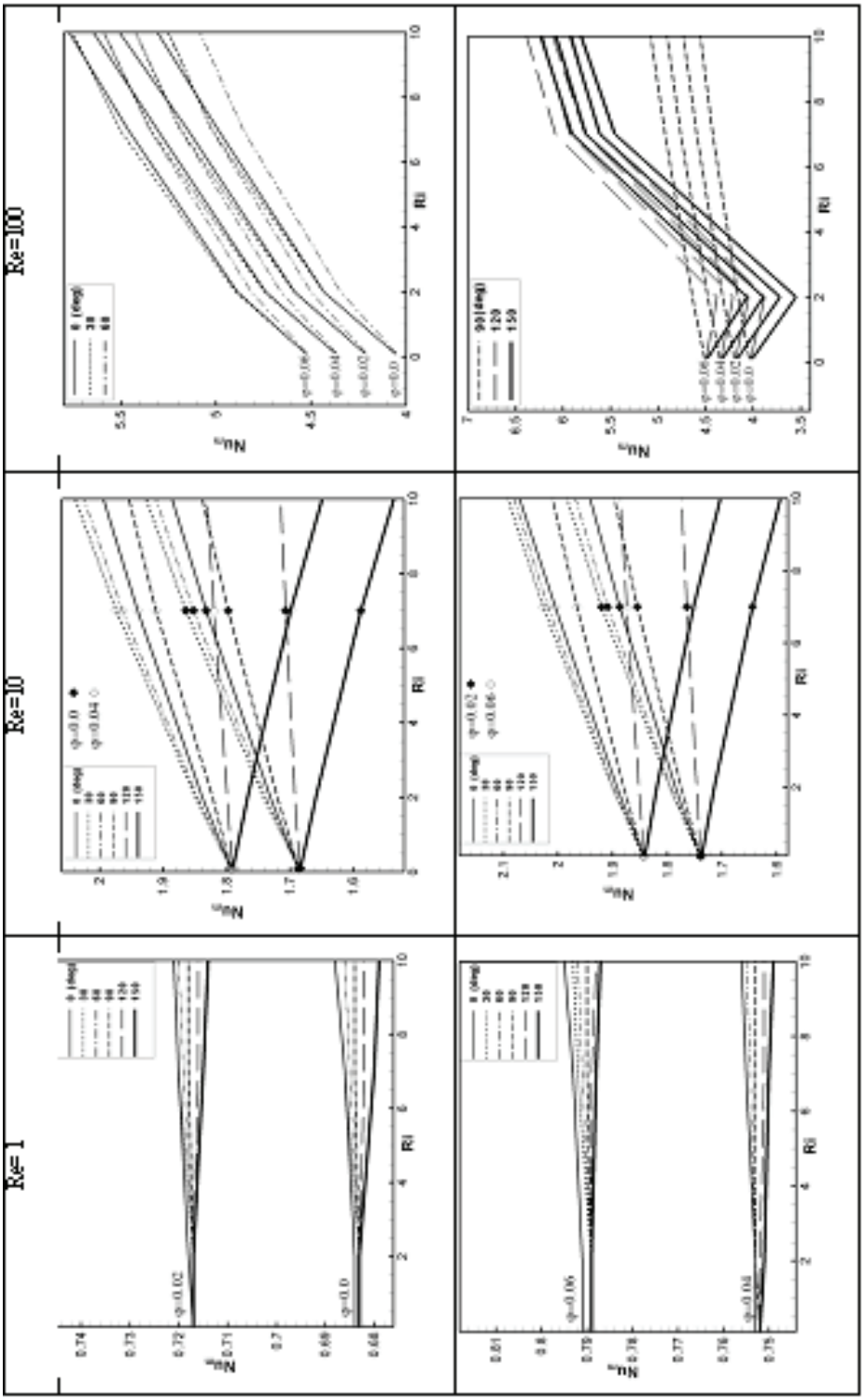

FIG. 6: Average Nusselt numbers at $\gamma = 0^{o}$ for all of the cases studied

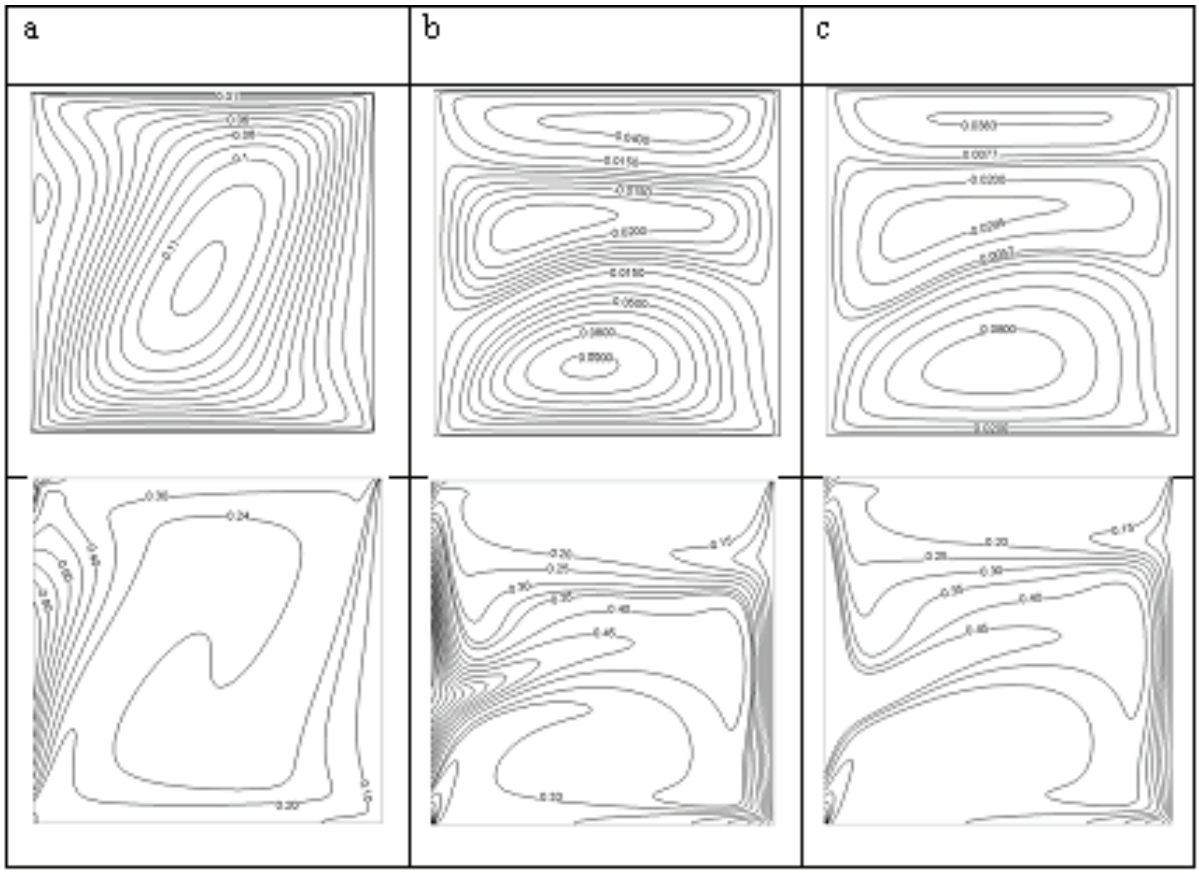

FIG. 7: Streamlines and isotherm lines for Re = 100, $\gamma = 150^{o}$, $\varphi = 0.06$: a) Ri = 2; b) Ri = 7; c) Ri = 10

6. CONCLUSIONS

In this study, mixed convection flows through a nanofluid in a square double lid-driven cavity with various inclination angles was carried out. The cavity was nonuniformly heated from the left, T_h, and cooled from the opposite wall. The top and the bottom moving walls were insulated. The study was conducted for the Richardson number 0.1 to 10, Reynolds number 1 to 100, while solid volume fractions (φ) of nanoparticles were altered from 0 to 0.06.

In view of the results obtained, the following findings may be summarized:

- By increasing the Reynolds number from 1 to 100, nanofluid moves faster in the horizontal direction and streamlines accede to the hot and cold surfaces and heat transfer increases because of the enhancement in the rate of flow passing near the hot and cold surfaces.
- By increasing the Re number from 1 to 100, a stronger flow field is produced in the cavity.
- When the Ri number is altered from 0.1 to 10, the conduction and natural convection increase.
- Because the buoyancy and shear forces are aiding each other for $\gamma = 30^{o}$, the intensity of streamlines increases near the walls, and the circulation in the cavity becomes stronger.
- Increment in φ generally causes a stronger circulation.

- With increase in the Re or Ri number, the isotherm lines get closer to the hot and cold walls.
- The temperature gradient increases especially near the cold wall as the heat transfer does.

Further studies aimed at elucidation of the precise nature of this flow regime would be of considerable interest. In addition, more investigations are called for in order to find out the reasons that lead to heat transfer deterioration in nanofluids. The extension of this study on the basis of previous works (Noorian et al., 2014a,b; Rezaei et al., 2015a,b; Semiromi and Azimian, 2010a,b,c; Semiromi and Azimian, 2012; Toghraie et al., 2016a,b; Toghraie and Azimian, 2009) affords engineers an opportunity for conducting simulations and experimental investigations.

REFERENCES

Akbari, O.A., Toghraie, D., and Karimipour, A., Impact of Ribs on Flow Parameters and Laminar Heat Transfer of Water–Aluminum Oxide Nanofluid with Different Nanoparticle Volume Fractions in a Three-Dimensional Rectangular Microchannel, *Adv. Mech. Eng.*, vol. **7**, no. 11, pp. 1687814015618155, 2015.

Akbari, O.A., Toghraie, D., and Karimipour, A., Numerical Simulation of Heat Transfer and Turbulent Flow of Water Nanofluids Copper Oxide in Rectangular Microchannel with Semi-Attached Rib, *Adv. Mech. Eng.*, vol. **8**, pp. 1–25, 2016.

Basak, T., Roy, S., Sharma, P.K., and Pop, I., Analysis of Mixed Convection Flows within a Square Cavity with Uniform and Nonuniform Heating of Bottom Wall, *Int. J. Thermal Sci.*, vol. **48**, pp. 891–912, 2009.

Brinkman, H.C., The Viscosity of Concentrated Suspensions and Solutions, *J. Chem. Phys.*, vol. **20**, pp. 571–581, 1952.

Esfe, M.H., Akbari, M., Karimipour, A., Afrand, M., Mahian, O., and Wongwises, S., Mixed-Convection Flow and Heat Transfer in an Inclined Cavity Equipped to a Hot Obstacle Using Nanofluids Considering Temperature-Dependent Properties, *Int. J. Heat Mass Transfer*, vol. **85**, pp. 656–666, 2015a.

Esfe, M.H., Arani, A.A.A., Rezaie, M., Yan, W.M., and Karimipour, A., Experimental Determination of Thermal Conductivity and Dynamic Viscosity of Ag–MgO/Water Hybrid Nanofluid, *Int. Commun. Heat Mass Transfer*, vol. **66**, pp. 189–195, 2015b.

Esfe, M.H., Karimipour, A., Yan, W.M., Akbari, M., Safaei, M.R., and Dahari, M., Experimental Study on Thermal Conductivity of Ethylene Glycol Based Nanofluids Containing Al_2O_3 Nanoparticles, *Int. J. Heat Mass Transfer*, vol. **88**, pp. 728–734, 2015c.

Esfe, M.H., Akbari, M., Toghraie, D., Karimipour, A., and Afrand, M., Effect of Nanofluid Variable Properties on Mixed convection Flow and Heat Transfer in an Inclined Two-Sided Lid-Driven Cavity with Sinusoidal Heating on Sidewalls, *Heat Transfer Research*, vol. **45**, pp. 409–432, 2014.

Eshgarf, H. and Afrand, M., An Experimental Study on Rheological Behavior of non-Newtonian Hybrid nano-Coolant for Application in Cooling and Heating Systems, *Exp. Thermal Fluid Sci.*, vol. **76**, pp. 221–227, 2016.

Karimipour, A., Esfe, M.H., Safaei, M.R., Semiromi, D.T., Jafari, S., and Kazi, S.N., Mixed Convection of Copper–Water nanoFluid in a Shallow Inclined Lid-Driven Cavity Using the Lattice Boltzmann Method, *Physica A: Statist. Mech. Appl.*, vol. **402**, pp. 150–168, 2014.

Karimipour, A., New Correlation for Nusselt Number of Nanofluid with $Ag/Al_2O_3/Cu$ Nanoparticles in a Microchannel Considering Slip Velocity and Temperature Jump by Using Lattice Boltzmann Method, *Int. J. Thermal Sci.*, vol. **91**, pp. 146–156, 2015.

Karimipour, A., Nezhad, A.H., Behzadmehr, A., Alikhani, S., and Abedini, E., Periodic Mixed Convection of a Nanofluid in a Cavity with Top Lid Sinusoidal Motion, *Proc. Inst. Mech. Eng., Part C: J. Mech. Eng. Sci.*, vol. **225**, pp. 2149–2160, 2011.

Karimipour, A., Nezhad, A.H., D'Orazio, A., Esfe, M.H., Safaei, M.R., and Shirani, E., Simulation of Copper–Water Nanofluid in a Microchannel in Slip Flow Regime Using the Lattice Boltzmann Method, *Eur. J. Mech. — B/Fluids*, vol. **49**, pp. 89–99, 2015.

Luo, W.J. and Yang, R.J., Multiple Fluid Flow and Heat Transfer Solutions in a Two-Sided Lid-Driven Cavity, *Int. J. Heat Mass Transfer*, vol. **50**, pp. 2394–2405, 2007.

Maxwell, J.C., *A Treatise on Electricity and Magnetism*, 2nd ed., Cambridge: Oxford University Press, pp. 435–441, 1904.

Nikkhah, Z., Karimipour, A., Safaei, M.R., Forghani-Tehrani, P., Goodarzi, M., Dahari, M., and Wongwises, S., Forced Convective Heat Transfer of Water/Functionalized multi-Walled Carbon Nanotube Nanofluids in a Microchannel with Oscillating Heat Flux and Slip Boundary Condition, *Int. Commun. Heat Mass Transfer*, vol. **68**, pp. 69–77, 2015.

Noor, D.Z., Kanna, P.R., and Chern, M.J., Flow and Heat Transfer in a Driven Square Cavity with Double-Sided Oscillating Lids in anti-Phase, *Int. J. Heat Mass Transfer*, vol. **52**, pp. 3009–3023, 2009.

Noorian, H., Toghraie, D., and Azimian, A.R., The Effects of Surface Roughness Geometry of Flow Undergoing Poiseuille Flow by Molecular Dynamics Simulation, *Heat Mass Transfer*, vol. **50**, no. 1, pp. 95–104, 2014a.

Noorian, H., Toghraie, D., and Azimian, A.R., Molecular Dynamics Simulation of Poiseuille Flow in a Rough nano Channel with Checker Surface Roughnesses Geometry, *Heat Mass Transf.*, vol. **50**, no. 1, pp. 105–113, 2014b.

Ouertatani, N., Cheikh, N.B., Beya, B.B., Lili, T., and Campo, A., Mixed Convection in a Double Lid-Driven Cubic Cavity, *Int. J. Thermal Sci.*, vol. **48**, pp. 1265–1272, 2009.

Oztop, H.F. and Dagtekin, I., Mixed Convection in Two-Sided Lid-Driven Differentially Heated Square Cavity, *Int. J. Heat Mass Transfer*, vol. **47**, pp. 1761–1769, 2004.

Patel, H.E., Sundararajan, T., Pradeef, T., Dasgupta, A., Dasgupta, N., and Das, S.K., A Micro-Convection Model for Thermal Conductivity of Nanofluids, *J. Physics*, vol. **65**, pp. 863–869, 2005.

Rezaei, M., Azimian, A.R., and Toghraie, D., Molecular Dynamics Study of an Electro-Kinetic Fluid Transport in a Charged Nanochannel Based on the Role of the Stern layer, *Physica A: Statistical Mechanics and its Applications*, vol. **426**, pp. 25–34, 2015a.

Rezaei, M., Azimian, A.R., and Semiromi, D.T., The Surface Charge Density Effect on the Electro-Osmotic Flow in a Nanochannel: A Molecular Dynamics Study, *Heat Mass Transf.*, vol. **51**, no. 5, pp. 661–670, 2015b.

Sivasankaran, S., Sivakumar, V., and Prakash, P., Numerical Study on Mixed Convection in a Lid-Driven Cavity with Nonuniform Heating on Both Sidewalls, *Int. J. Heat Mass Transfer*, vol. **53**, pp. 4304–4315, 2010.

Semironi, D.T. and Azimian, A.R., Molecular Dynamics Simulation of Liquid–Vapor Phase Equilibrium by Using the Modified Lennard-Jones Potential Function, *Heat Mass Transf.*, vol. **46**, no. 3, pp. 287–294, 2010a.

Semironi, D.T. and Azimian, A.R., Nanoscale Poiseuille Flow and Effects of Modified Lennard–Jones Potential Function, *Heat Mass Transf.*, vol. **46**, no. 7, pp. 791–801, 2010b.

Semironi, D.T. and Azimian, A.R., Molecular Dynamics Simulation of Nonodroplets with the Modified Lennard-Jones Potential function, *Heat Mass Transf.*, vol. **47**, no. 5, pp. 579–588, 2010c.

Semiromi, D.T. and Azimian, A.R., Molecular Dynamics Simulation of Annular Flow Boiling with the Modified Lennard–Jones Potential Function, *Heat Mass Transf.*, vol. **48**, pp. 141–152, 2012.

Tiwari, R.K. and Das, M.K., Heat Transfer Augmentation in a Two-Sided Lid-Driven Differentially Heated Square Cavity Utilizing Nanofluids, *Int. J. Heat Mass Transfer*, vol. **50**, pp. 2002–2018, 2007.

Toghraie, D., Alempour, S.M.B., and Afrand, M., Experimental Determination of Viscosity of Water Based Magnetite Nanofluid for Application in Heating and Cooling Systems, *J. Magnetism and Magnetic Materials*, vol. **417**, pp. 243–248, 2016a.

Toghraie, D., Chaharsoghi, V.A., and Afrand, M., Measurement of Thermal Conductivity of ZnO–TiO_2/EG Hybrid Nanofluid, *J. Therm. Anal. Calorim*, vol. **125**, no. 1, pp. 527–535, 2016b.

Toghraie, D. and Azimian, A.R, Molecular Dynamics Simulation of Liquid-Vapor Interface on the Solid Surface Using the GEAR'S Algorithm, *Int. J. Chem. Molecular Eng.*, vol. **3**, no. 9, pp. 453–457, 2009.

Wahba, E.M., Multiplicity of States for Two-Sided and Four-Sided Lid-Driven Cavity flows, *Computers & Fluids*, vol. **38**, no. 2, pp. 247–253, 2009.

Xuan, Y. and Li, Q., Heat Transfer Enhancement of Nanofluids, *Int. J. Heat Fluid Flow*, vol. **21**, pp. 58–64, 2000.

Zarringhalam, M., Karimipour, A., and Toghraie, D., Experimental Study of the Effect of Solid Volume Fraction and Reynolds Number on Heat Transfer Coefficient and Pressure Drop of CuO–Water Nanofluid, *Exp. Thermal Fluid Sci.*, vol. **76**, pp. 342–351, 2016.